J Electroceram (2009) 23:25–36
DOI 10.1007/s10832-008-9516-0

Effect of time and polarization on kinetics of the oxygen electrode reaction at an Au | YSZ interface

P. Tomczyk · S. Żurek · M. Mosiałek

Received: 25 June 2006 / Accepted: 18 April 2008 / Published online: 26 May 2008

Abstract The oxygen electrode reaction at the interface gold | yttria stabilized zirconia was investigate using microelectrodes by chronoamperometry and electrochemical impedance spectroscopy, with emphasis put on effect of prolonged polarization of the electrode. Two interesting phenomena were observed: (a) generally, the long-lasting negative polarization resulted in a slow monotonous decrease of the current flowing through the electrode, (b) the reaction mechanism was less complicated for the polarized then unpolarized electrodes, which resulted in a relatively simply equivalent circuit used for modelling the former ones. On the basis of the data obtained, the apparent exchange currents normalized vs. the three phase boundary length and Tafel slopes were determined. The methods of determining the three phase boundary length were discussed. The reconnaissance data obtained for the Pt microelectrode are also reported.

Keywords Oxygen electrode · Au microelectrode · YSZ · Three phase boundary · Exchange current

P. Tomczyk (✉)
Faculty of Fuels and Energy,
AGH—University of Science and Technology,
al. Mickiewicza 30,
30-059 Krakow, Poland
e-mail: ptomczyk@uci.agh.edu.pl

S. Żurek · M. Mosiałek
Department of Electrochemical Oxidation of Fuels,
Institute of Physical Chemistry
of the Polish Academy of Sciences,
ul. Kasprzaka 44/52,
01-224 Warsaw, Poland

1 Introduction

For over 50 years, yttria stabilized zirconia (YSZ) is still believed to be the most suitable electrolyte for use in oxygen sensors, solid oxide fuel cells (SOFCs) and water vapour electrolysers despite strenuous efforts aimed at finding other, superior ionic solid for these applications. This opinion has been formed due to the high ionic conductivity and stability of YSZ [1–5].

The thermodynamics of yttria stabilized zirconia is well understood for decades. However, a controversy still persists over the mechanism and kinetics of processes occurring at an interface electrode | YSZ electrolyte [6–10]. This problem is of key importance for the SOFCs, where apart from the ohmic drop, slow kinetics of electrode processes is a source of significant energy losses.

In all types of fuel cells, porous electrodes are used to provide high density of current drawn from the cell under load. One of the possible reasons for unsatisfying understanding of electrode reactions in the SOFCs with YSZ electrolyte is the fact that majority of studies has been made, by an analogy to the state-of-the-art fuel cell, on porous electrodes with complex and difficult to determine structure and geometry. To avoid problems associated with porous electrodes at solid state electrolytes, a number of researchers have applied a concept of microelectrodes, well known from liquid electrochemistry. In solid state electrochemistry, the microelectrodes were frequently exploited in polymer electrolytes [11–14] whereas they were less commonly employed in ionic solids [15–18]. Use of microelectrodes has a number of benefits: (1) facilitates the investigation of charge transfer reaction, (2) enables to scan properties of electrode surface and electrolyte and (3) reduces the effect of ohmic drops, which affects the results of measurements in low-conducting electrolytes.

Two types of microelectrodes are generally utilized in solid state ionics: sharp needles directly pressed onto the sample and dense film dots deposited by either pulsed laser deposition or lithographic pattering. Unfortunately, even in the case of microelectrodes with well defined dimensions and structures prepared by the latter methods, the results obtained are frequently poorly reproducible. One of the reasons for this behaviour can arise from inhomogeneous surface properties of the electrolyte, whereas the other may result from an irreversibility of processes produced by a DC-bias applied, intentionally or unintentionally, to the electrodes.

During fuel cell operation under load, the cathodes are polarized with overpotentials $|\Delta\eta|$, which often exceed 0.3 V for thousands of hours. There are several reports in the literature that the electrical efficiency of SOFC with LSM or LSCo cathodes increases significantly in the first several hours of loading. The improvement of fuel cell characteristics is confined to electrode | electrolyte interface, namely to: (1) microstructural changes [19], (2) removing of passive species [20], (3) enhancing performance of the oxygen exchange surface reaction [21], (4) formation of oxygen vacancies at the LSM surface [22], (5) reduction of contacting resistance [23] and (6) acceleration of oxygen surface dissociation and diffusion [24].

In the conditions relevant to the SOFC operation, the enhanced currents were also observed for gold electrodes on YSZ; this behaviour was attributed to stoichiometric changes of the electrolyte induced by the high applied voltage [25–26]. Presumably, the so called, irreversible behaviour of Pt microelectrodes on YSZ surface [27–29], may also be associated with the similar changes of electrolyte structure.

Our work is aimed at an elucidation of effects of prolonged polarization on the current response of metallic microelectrode. Since dense, metallic microelectrode constrains to occur significant reactions at three phase boundaries and therefore corresponds, in a certain sense, to a single particle of porous electrode, such studies are worth to be performed. The emphasis was put on effect of negative polarization of the electrode, because the cathodic process predominantly affects the current–voltage characteristics of the cell. This article concentrates at the processes occurring at an Au | YSZ interface because of the following reasons: (1) the enhancement of the currents was already reported at high biases for the gold electrodes, which were formed as inter-digitated strips [25]. We observed that the similar effect occurs for the quasi-point Au electrode polarized with the significantly smaller overpotentials; (2) to date published papers described, the so called, irreversible behaviour of Pt microelectrodes [27–29]. It is of interest to check if this behaviour can be correlated with the enhancement of currents observed for the micro-electrodes made of other materials than Pt. The present work reports the data obtained at an interface Au | YSZ, whereas the similar investigations for Ag and Pt electrodes are now under way; (3) well defined contact between Au and YSZ electrolyte are formed easier than in the case of Ag and Pt (silver and platinum are more plastic and more rigid than gold in the measurement temperature, respectively). Therefore, to acquire experience in the optimal conditions of the measurement, Au was chosen for the first experimental series. Nevertheless, preliminary results obtained with the Pt microelectrode are also presented in this paper for comparison.

2 Experimental

The YSZ electrolyte had a form of disk of 10 mm diameter and 3 mm thickness. The sintering process was performed at 1570 °C using zirconia powder doped with 8 mol% of yttria. The powder characteristics were as follow: ca. 10 m^2g^{-1} surface area, below 0.5 μm average particle size, ca. 98% of theoretical sinterability at 1300 °C and over 99.95% purity. After sintering, the surface of the disk was polished with a 3000 waterproof alumina abrasive paper and afterwards 1 μm diamond paste.

The construction of the experimental, three electrode measurement system is presented in Fig. 1. Two microelectrodes were made from Au and Pt wires of 0.3 mm diameter. The wire was treaded throughout two holes of alumina bead forming a semicircle. During the experiment, these electrodes were alternatively used as working and reference electrode. The electrodes and disk were assembled inside an alumina holder and gripped together due to action of springs with a force of about 0.5 N. A counter electrode, in the form of platinum ring made from a wire of diameter 0.5 mm, was located in a furrow grooved around the side wall of the disk. The contact between the platinum ring and YSZ electrolyte was improved with platinum paste, which was smeared at inside walls of the furrow. The holder with electrochemical system of electrodes and electrolyte was then placed inside an alumina envelope, which provided a gas-tight separation from the outer

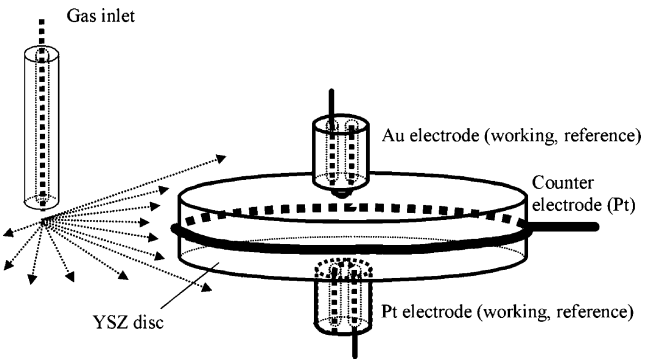

Fig. 1 Schematic draw of the electrochemical measurement system

Table 1 Conductivities of YSZ (8–10% Y_2O_3) at 800 °C, determined by various authors.

Reference	σ_{el}/ohm^1 cm $^{-1}$
[2]	0.028
[4]	0.020
[37]	0.014
[38]	0.010
[39]	0.020

atmosphere. Finally, the whole system was located in a horizontal electric furnace.

An inlet of the gases was situated a few millimeters from the side wall of the disk providing the gases to flow directly to the electrodes. A set up of gas flow controllers allowed to control the composition and flow rates of gases introduced into the cell. The experiments were performed for different contents of O_2 in a mixture of O_2+Ar, equivalent to the oxygen partial pressures p_{O2}=0.01, 0.1 and 1.0 bar. The flow rate of the gases into the electrochemical cell was 20 ml/min.

Before the experiment, the cell was heated to 950–1000 °C and held about 1 h at this temperature. In these conditions, gold and platinum became soft and the microelectrodes, pressed by the springs to the disk, increased contact areas between the metal and electrolyte. After heating the cell at 950–1000 °C, the temperature was decreased to the measurement temperature and the system was left for 24 h to stabilize under the flow of O_2+Ar mixture. The experiments were performed at 600, 700 and 800 °C.

The chronoamperometric (CA) and electrochemical impedance spectroscopy (EIS) techniques were used in the measurements. Due to long-term effects of electrode polarization, the dependences of the current on the time of polarization were recorded in durations of at least 15 h for the Au microelectrodes and 3.5 h in the reconnaissance experiments for the Pt microelectrodes. In the CA experiments, the microelectrodes were polarized from the rest potential down to –0.3 V with an increment of 0.05 V. Between the consecutive polarizations, the electrode was left relaxing for ca. 30 h. To get additional information, the EIS was applied to determine and characterize the impedance of the electrode before the polarization and at the end of the potential step.

The electrochemical measurements were performed with an IM5D Impedance Spectrum Analyser, a product of Zahner Elektrik, Kronach. The CA dependences of the current on the time were recorded using PVI software, provided by the producer. Generally, the frequency range used in the EIS measurements was 0.02 to 100,000 Hz. The amplitude of sinusoidal voltage signal was 10 mV. For analysis of the impedance data, a program based on a complex non-linear regression least-squares (CNRLS) fit was used. This program was also provided by the producer.

3 Results and discussion

3.1 Determining the length of three phase boundary

In the circumstances of our experiment, i.e. for the metallic electrode in a direct contact with the solid state ionic electrolyte, the electrode reactions occur exclusively at the three phase boundary (TPB). Two procedures, which were used for determining the TPB length in the series of measurements performed with the same Au microelectrode at 800 °C, are described below. The similar measures were applied for the other experimental series.

3.1.1 Geometrical estimation of the TPB length

After completing the experiment and disassembling the cell, the electrodes were examined with a scanning microscope. The flattened part of metal surface at the image corresponded to the area that was in a direct contact with the electrolyte. It was elliptically shaped because side wall of the wire was deformed by pressing to the electrolyte. The TPB length was estimated by a direct geometric measurement of the perimeter of the flattened part of electrode. It was equal to 2.60 mm.

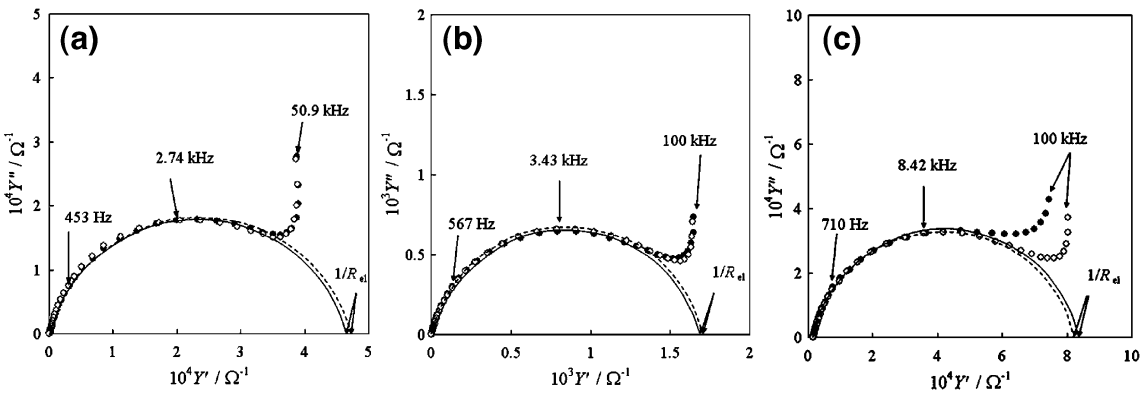

Fig. 2 Complex admittance plots. (**a**) Au microelectrode, 700 °C, p_{O2}=0.1 bar; (**b**) Au microelectrode, 800 °C, p_{O2}=0.1 bar; and (**c**) Pt microelectrode, 800 °C, p_{O2}=0.1 bar

3.1.2 Estimation of the TPB length from the electrochemical measurements

The TPB length was also determined using the Newmann equation, which could be written for a perfectly circular, metallic microelectrode in the form [30]:

$$R_{el} = \frac{\pi}{2l^{\circ}_{TPB}\sigma_{el}} \quad (1)$$

where R_{el} is the electrolyte resistance determined by the impedance spectroscopy, σ_{el} is the specific conductivity of the electrolyte and is the three phase boundary length of circular electrode. However, the microelectrodes used in our experiments were not circular but elliptical, hence their TPB boundary lengths l_{TPB} have to be enlarged by the factor γ:

$$\gamma = 0.75(\zeta + 1) - 0.5\sqrt{\zeta} \quad (2)$$

$$l_{TBP} = \gamma l^{\circ}_{TPB} \quad (3)$$

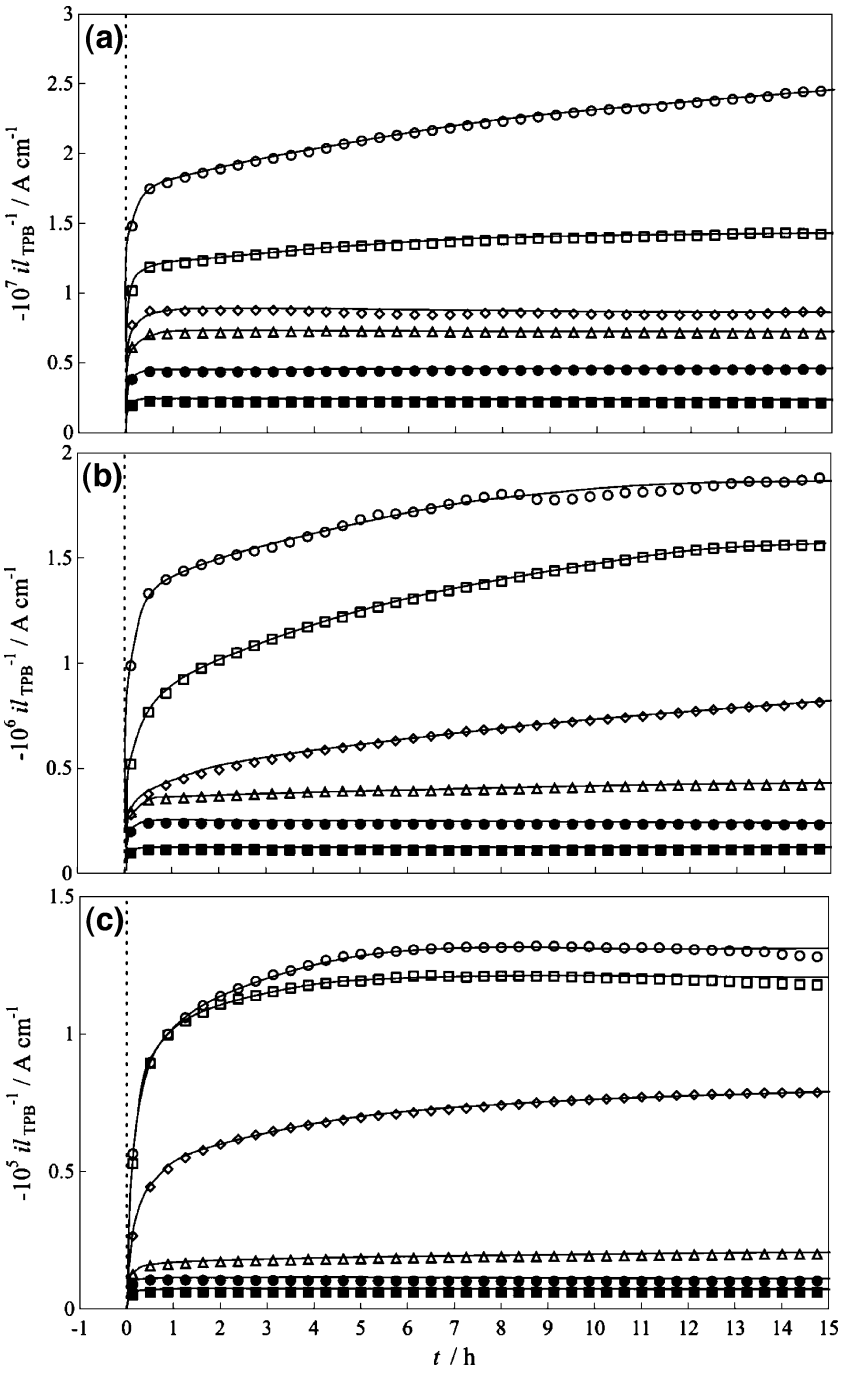

Fig. 3 Dependences of the currents normalized vs. the TPB length on the time of polarization. Au microelectrode, 800 °C. Polarizations: *filled square* −0.05 V; *filled circle* −0.1 V; *unfilled triangle*: −0.15 V; *unfilled diamond* −0.2 V; *unfilled square* −0.25 V and *unfilled circle* −0.3 V. (**a**) p_{O2}=0.01 bar, (**b**) p_{O2}=0.1 bar and (**c**) p_{O2}=1 bar

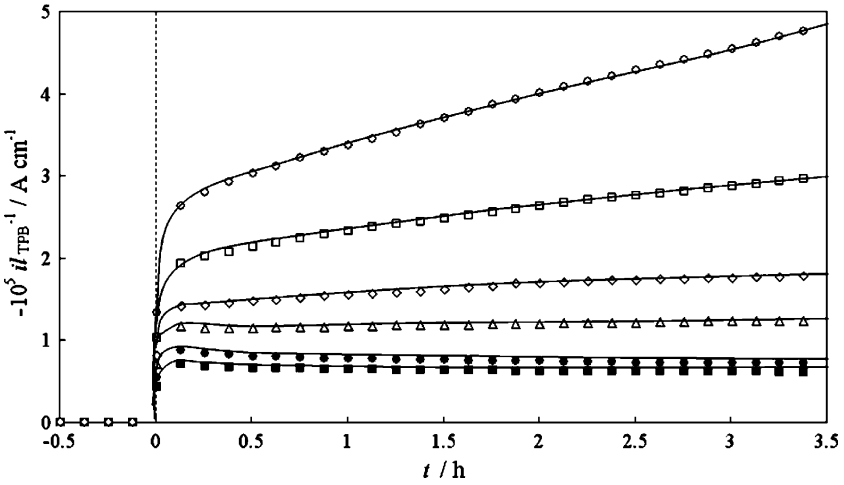

Fig. 4 Dependences of the currents normalized vs. the TPB length on the time of polarization. Pt microelectrode, 800 °C. Notations as in Fig. 3

where $\xi=a/b$ and a, b are the semimajor and semiminor axes of ellipse, respectively. For all the electrodes used in our experiments, the deformation parameter $\xi\cong 2.9$. Thus, as can be calculated from Eq. (2), the corrective factor $\gamma\cong 2.1$. More detailed considerations regarding this evaluation can be found in our earlier paper [31].

To estimate the TPB length l_{TPB} from Eqs. (1)–(3), the resistance R_{el} and specific conductivity of the electrolyte σ_{el} must be known. For our electrolyte sample, $\sigma_{el}=0.020$ $\Omega^{-1}cm^{-1}$ was determined from the EIS measurement. In this measurement, large porous Pt electrodes, considered to behave reversibly, were deposited on opposite sides of the YSZ disk. The conductivity data of $ZrO+(8–10\%)Y_2O_3$ at 800 °C, obtained by various authors, are presented in Table 1 for comparison. It should be emphasized that the scatter of the data presented in Table 1 occurs likely due to different conditions of the sample preparation (temperature, time of sintering) and properties of reagents (particle size, purity, sinterability).

R_{el}, the electrolyte resistance, was estimated from the complex admittance plots such as these presented in Fig. 2. For the data presented in Fig. 2, it is relatively easy to fit a semicircle, which represents polarization admittance of the oxygen electrode. The right crossing points of the semicircle with the Y′ axis can be attributed to the total admittance of the electrolyte. As can be seen in Fig. 2, the admittance of the electrolyte $1/R_{el}$ is independent of the duration of the experiment and polarization of the electrode. Determining the electrode resistance from the complex impedance plots appeared to be less precise because of a small number and uncertainty of experimental points in the required range of high frequencies [31]. For the considered experimental series performed at 800 °C with the Au microelectrode, R_{el}=606–622 Ω.

By inserting into Eqs. (1–3) $\gamma=2.1$, $\sigma_{el}=0.020$ Ω^{-1} cm^{-1} and R_{el}=606–622 Ω, the TPB boundary lengths was calculated to be equal l_{TPB}=2.65–2.72 mm. This value agree well with the TPB length determined from the geometrical measurement, which was described in Section 3.1.1. Therefore, to avoid the difficulties related to the geometrical determination of l_{TPB} for each single electrode, we decided to used in our further calculations the l_{TPB} value determined according to the procedure described Section 3.1.2. This procedure allowed us also to detect immediately any change in geometry of the electrochemical system during the experiments lasting at least a couple of weeks.

Because Pt is less plastic than Au at elevated temperatures, the TPB lengths of the Pt electrodes (1.32–1.45 mm) were almost twice lower than these of the Au electrodes in the same conditions of the experiment (800 °C, preheated to 950–1000 °C).

3.2 Current vs. time dependences for the oxygen reduction

Typical CA dependences of the currents flowing through the Au electrode at different negative polarizations are shown in Fig. 3. They were determined at 800 °C for the three partial pressure of oxygen p_{O2}=0.01, 0.1 and 1 bar. The currents in this figure were normalized vs. the TPB lengths, determined according to the procedure described in

Table 2 The apparent exchange currents normalized vs. the TPB length and Tafel slopes calculated from the CA measurements for the Au | YSZ and Pt | YSZ interfaces.

Electrode	Temperature/°C	p_{O2}/bar	$-i_0 l_{TPB}^{-1}$/Acm^{-1}	αn
Au	600	0.1	1.4e-8	0.5
	700	0.01	9.2e-9	0.7
		0.1	4.2e-8	1.0
		1.0	1.8e-7	0.9
	800	0.01	5.4e-8	0.8
		0.1	1.7e-7	1.0
		1.0	4.3e-7	1.1
Pt	800	0.1	3.1e-5	0.8

Section 3.1.2. Because the stable values of the currents were approached very slowly, especially at lower potentials, the experiments lasted at least 15 h. There are six curves presented for the each partial pressure of oxygen; the curves were recorded at the potentials −0.05, −0.1, −0.15, −0.2, −0.25 and −0.3 V. For the gold electrodes, the analogous dependences of the current on the polarization time were also determined at 600 °C (p_{O2}=0.1 bar) and 700 °C (p_{O2}= 0.01, 0.1 and 1.0 bar).

These dependences show the following characteristics:

(a) as it was mentioned before, long time was necessary for the currents to stabilize when the electrode was polarized with a steady negative potential lower than −0.15 V. In these cases, the character of current-time dependences had generally an asymptotic character. For the higher potentials, the currents approached stable values much faster, after 1–3 h of the polarization;

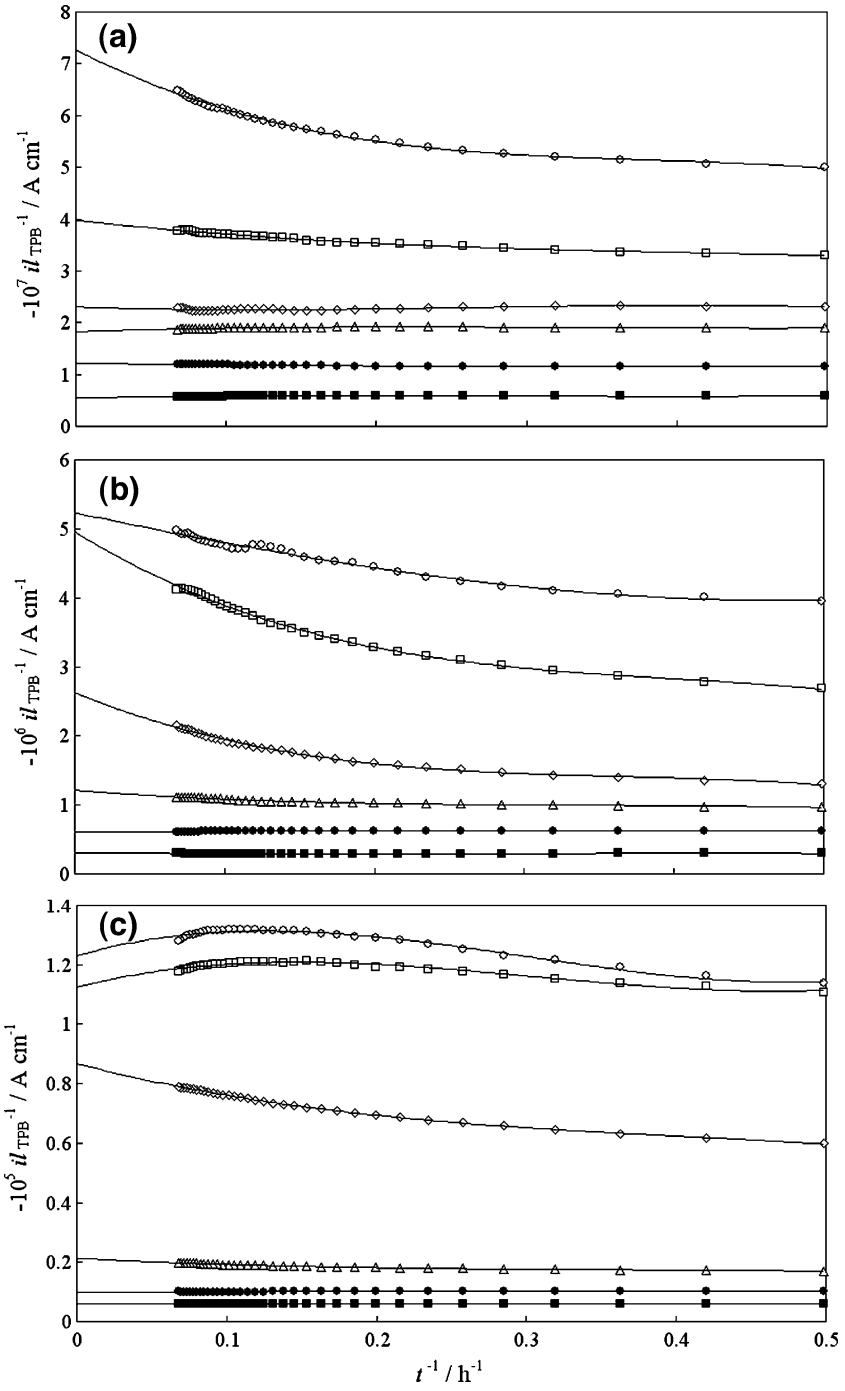

Fig. 5 Dependences of the normalized currents on the inverse of polarization time. The *solid lines* represent the fits of Eq. (4) to the experimental points. Conditions of the experiment and notations as in Fig. 3

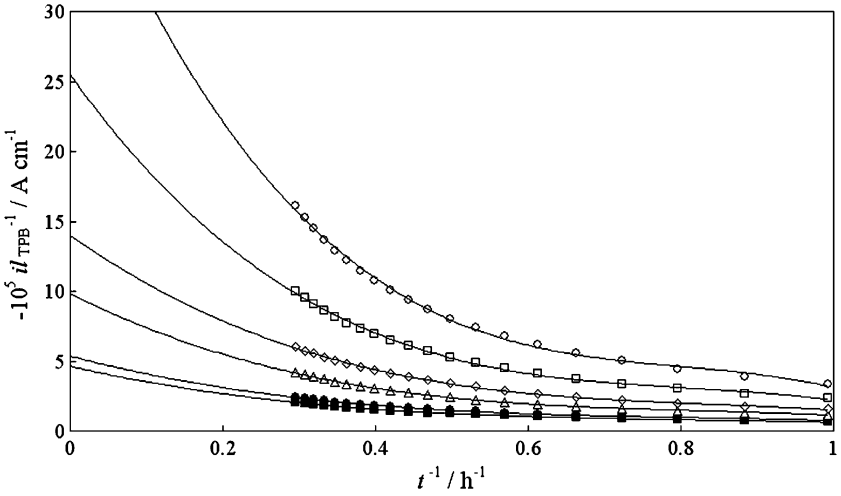

Fig. 6 Dependences of the normalized currents on the inverse of polarization time. The *solid lines* represent the fits of Eq. (4) to the experimental points. Conditions of the experiment and notations as in Fig. 4

(b) generally, the absolute currents had a tendency to increase monotonically with the time. Only at 700 °C and p_{O2}=0.01 bar, after abrupt increase just at the moment of switching the polarization on, the currents gradually decreases.

The similar dependences obtained for the Pt microelectrode under p_{O2}=0.1 bar at 800 °C are presented in Fig. 4. These measurements had a reconnaissance character, therefore the dependences were recorded in much shorter time of 3.5 h. The absolute normalized currents il_{TPB}^{-1}, which flowed through the Au electrode, were distinctly lower than these flowing through the Pt electrode in the same conditions of the experiment.

The increase of absolute value of current with the time during the CA experiments coincidences with the improvement of SOFC characteristics, described in the introduction to this article. Such a phenomenon is quite rare and therefore may be helpful to identify the mechanism of oxygen electrode in YSZ. In the case of a coupled catalytic reaction with a quasi-reversible or irreversible charge transfer, one may expect asymptotic grow of CA current. Unfortunately, no theoretical treatment of this scheme for a step-like polarization was performed, in contrast to, for example, linear scan voltammetry [32]. While the charge transfer in our case should rather be considered as a quasi-reversible process, an asymptotic approach to a steady state, non-zero current in CA experiments is also characteristic for a catalytic reaction following a reversible electron transfer, E_rC' [33–35]. An enhancement of reaction zone by a DC bias postulated in the literature [25, 26], although proceeds with different mechanism, may lead to similar effects.

Generally, the SOFCs are designed to operate in thousands of hours, therefore we believe that long-term effects of the polarizations are very important for practical reasons. So as, not to disregard these effects, an attempt

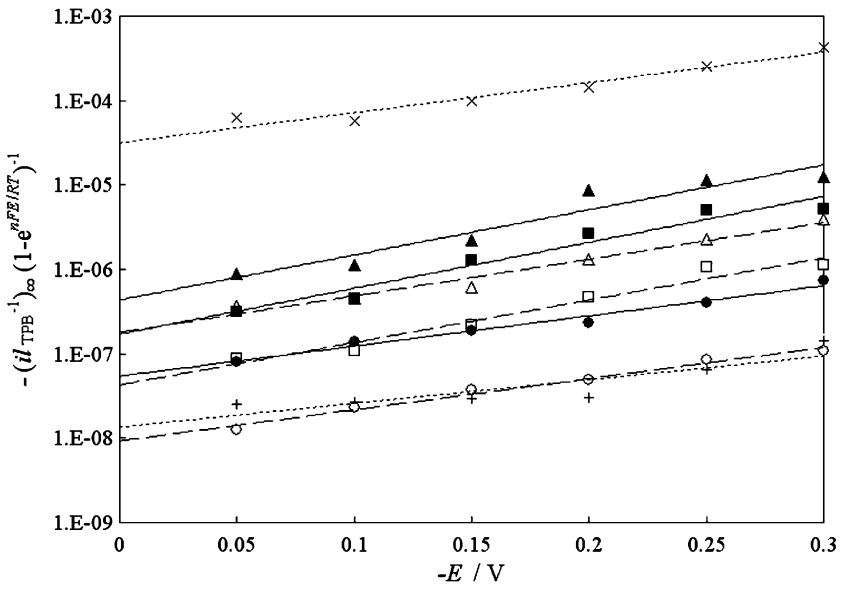

Fig. 7 Allen–Hickling plots for the normalized currents approximated to infinitely long time of polarization. *plus sign* Au microelectrode, 600 °C, p_{O2}= 0.1 bar; *unfilled circle*, *unfilled square*, *unfilled triangle* Au microelectrode, 700 °C, p_{O2}=0.01, 0.1 and 1 bar, respectively; *filled circle*, *filled square*, *filled triangle* Au microelectrode, 800 °C, p_{O2}=0.01, 0.1 and 1 bar, respectively and *multiplication sign* Pt microelectrode, 800 °C, p_{O2}=0.1 bar

was made to estimate the asymptotic values of the normalized currents $\left(il_{\mathrm{TPB}}^{-1}\right)_{\infty}$, which corresponded to their values after infinitely long time of the polarization.

So as, not to disregard these effects, an attempt was made to estimate the asymptotic values of the normalized currents $\left(il_{\mathrm{TPB}}^{-1}\right)_{\infty}$, which corresponded to their values after infinitely long time of the polarization.

To determine $\left(il_{\mathrm{TPB}}^{-1}\right)_{\infty}$, we fitted the parameters of Eq. (4)

$$il_{\mathrm{TPB}}^{-1} = \left(il_{\mathrm{TPB}}^{-1}\right)_{\infty} \pm const_1/t \pm const_2/t^2 \pm const_3/t^3 \quad (4)$$

to the experimental points with the least squares method. The polynomian (4) allows to estimate even complicated form of the dependence $il_{\mathrm{TPB}}{}^{-1}$ vs. t; its limiting value is equal to $\left(il_{\mathrm{TPB}}^{-1}\right)_{\infty}$ for $t \to \infty$. To reveal the character of dependences (4), they were shown in the coordinates $il_{\mathrm{TPB}}{}^{-1}$ vs. $1/t$ in Figs. 5 and 6 for the data presented in Figs. 3 and 4, respectively. The $\left(il_{\mathrm{TPB}}^{-1}\right)_{\infty}$ values correspond to the intercepts of dependences (4). To make the fitting procedure more reliable for long durations of the polarizations, the initial points, recorded at times shorter than 2 h for the Au electrodes and 1 h for the Pt electrodes, were passed over. Of course, for these CA currents, which stabilize soon since switching the polarization on (as it occurs frequently for $E>-0.15$ V), the $const_1$, $const_2$ and $const_3$ in Eq. (4) approaches values close to zero

The Allen–Hickling plots [36] of $\log\left\{\left(il_{\mathrm{TPB}}^{-1}\right)_{\infty}\Big/[1-\exp(nFE/RT)]\right\}$ vs. the polarization potential for the Au and Pt electrodes are presented in Fig. 7. $n=2$ was assumed, F, R and T are the Faraday constant, molar gas constant and temperature, respectively. The calculated values of the apparent exchange currents normalized vs. the TPB length and αn products, the so called Tafel slopes, are given in Table 2.

As can be noted, the normalized apparent exchange currents increase with increasing temperature and partial pressure of oxygen. Although the measurements with the Pt microelectrode had only preliminary character, it is distinctly seen that Pt is much better electrocatalyst for the oxygen reduction than Au. The scatter of the calculated Tafel slopes is relatively large, which may result from a poor reproducibility of data obtained at microelectrodes in solid ionics, "memory" effect and peculiar behaviour of the system. However, with some caution, one may argue that the calculated Tafel slopes are similar for all the considered cases, i.e. the similar mechanism of the oxygen reaction

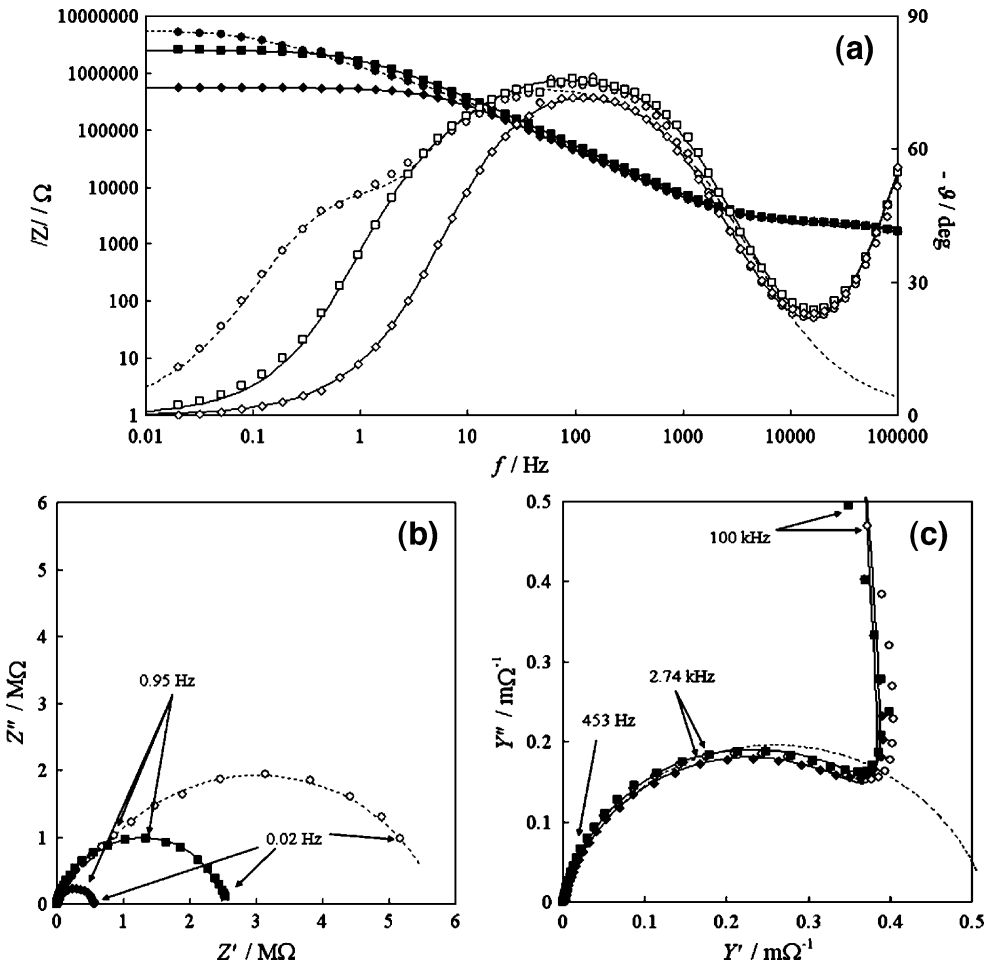

Fig. 8 Bode (**a**), complex impedance (**b**) and complex admittance (**c**) plots for the Au microelectrode at 700 °C under p_{O2}=0.1 bar. Polarizations: *unfilled circle*, *filled circle* 0 V; *unfilled square*, *filled square* −0.15 V and *unfilled diamond*, *filled diamond* −0.3 V. *Lines* correspond to the responses of the equivalent circuit shown in Fig. 10 fitted by the CRNLS method to the experimental points

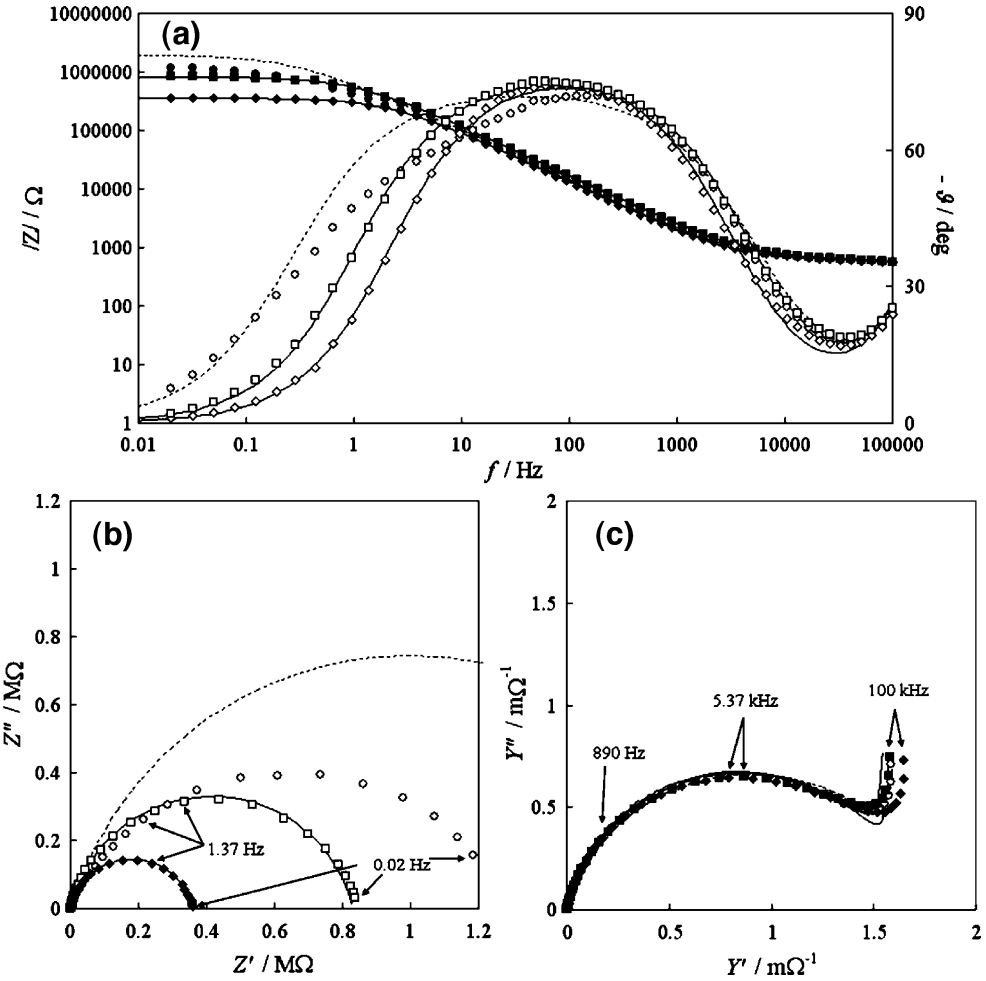

Fig. 9 Bode (**a**), complex impedance (**b**) and complex admittance (**c**) plots for the Au microelectrode at 800 °C under p_{O2}=0.1 bar. Notations as in Fig. 8

occurs independently of the oxygen partial pressure and material of electrode. Under this assumption, the average value of the Tafel slope for all the data presented in Table 2 was calculated to be equal to $(\alpha n)_{av}$= 0.85±0.19.

3.3 Effect of polarization on the impedance of the system

The EIS characteristics of the polarized electrodes were always measured at the end of the polarization step, just after recording the CA response, i.e. ca. 15 h since switching the polarization on. Then the electrode was left relaxing at the "open circuit" potential for about 30 h until the subsequent potential step was applied. Before the CA measurement, the EIS characteristics of unpolarized electrode were also recorded and evaluated. Indeed, we observed the "memory" effects of the polarization on the EIS characteristics even after 30 h relaxation of the electrode. The polarization was lower the effect was higher. To minimize the influence of this phenomenon on the EIS response, the potential of the following polarization step was always managed to be lower than the preceding one.

Typical Bode, complex impedance and complex admittance plots for the unpolarized and polarized Au microelectrodes at 700 and 800 °C under p_{O2}=0.1 bar are shown in Figs. 8 and 9. The lines in these figures correspond to the responses of the relatively simple equivalent circuit pictured in Fig. 10. A CRLNS fit to the experimental points was used to find the parameters of the circuit elements. Only for the polarized Au electrodes the

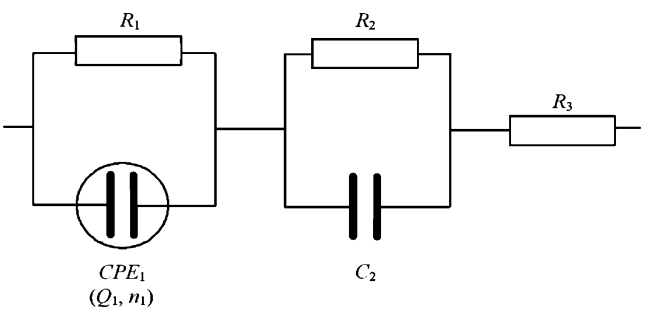

Fig. 10 Equivalent circuit used for modelling the polarized Au microelectrodes

experimental points were well approximated by the response of the equivalent circuit (solid lines in Figs. 8 and 9). It appeared also that the R_2 values corresponded to the electrolyte resistance R_{el}, estimated from the admittance plots presented in Fig. 2. Unfortunately, neither the unpolarized Au nor Pt electrodes could be simulated by the equivalent circuit shown in Fig. 10. In the range of either high or low frequencies, the large deviations of the fitted responses from the experimental points were distinctly observed (dotted lines in Figs. 8 and 9 for the Au unpolarized electrodes). This shows that some phenomena, occurring at the unpolarized Au electrode, could be eliminated by applying negative polarization.

The dependences of the fitted element parameters of the equivalent circuit on the potential of polarized Au electrode at 800 °C are presented in Fig. 11. As can be seen, all the parameters remain virtually constant in the whole range of applied potentials except the polarization resistance R_1. The same behaviour is observed at 700 °C. This observation emphasizes a crucial role of charge transfer in the oxygen electrode reaction at the Au | YSZ interface, apart from the phenomenon that produces the increase of the absolute CA currents with the time of polarization (see Section 3.2). In the discussion of the CA data in Section 3.2, the effect of the latter phenomenon was taken into account by estimation of $\left(il_{\mathrm{TPB}}^{-1}\right)_{\infty}$.

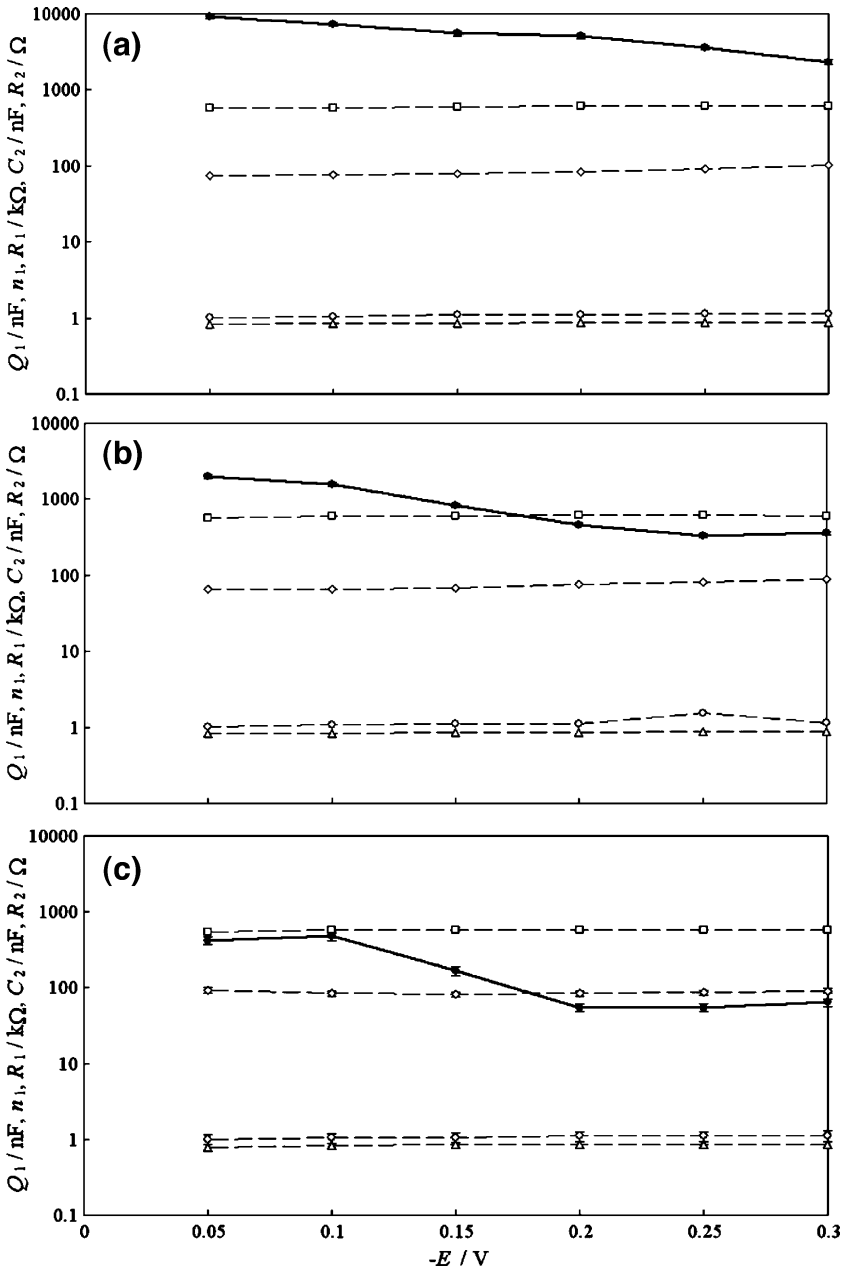

Fig. 11 Dependences of the fitted parameters of the equivalent circuit shown in Fig. 10 on the potential of polarization. *unfilled diamond* $Q1$, *unfilled triangle* $n1$, *filled circle* $R1$, *unfilled circle* $C2$ and *unfilled square* $R2$. Au microelectrode at 800 °C under (**a**) p_{O2}=0.01 bar, (**b**) p_{O2}=0.1 bar and (**c**) p_{O2}= 1 bar

However, let us assume that the process is exclusively controlled by a charge transfer and the electrode, represented by the equivalent circuit pictured in Fig. 10, is polarized with a steady potential. Then:

$$R_1 = [\mathrm{E} - i(\mathrm{R}_2 + \mathrm{R}_3)]/i \quad (5)$$

where

$$i = i_0 \exp(-\alpha n FE/RT)[1 - \exp(nFE/RT)] \quad (6)$$

The R_1 values calculated from Eqs. (5) and (6) and these determined by the CNRLS fit are compared in Fig. 12. In the calculations we used the apparent exchange current i_0 and αn=0.85 determined from the CA measurements (Table 2), R_2 (700 °C)=2.22 kΩ, R_2 (800 °C)=567 Ω, R_3=0 Ω and n=2. As can be seen, a relatively good agreement between the fitted and calculated values of R_1 is observed for the smallest polarizations, i.e. above –0.15 V. At the lowest partial pressures of oxygen, p_{O2}=0.01 bar, at least the character of dependences estimated from Eqs. (5) and (6) and determined from the EIS measurements, remains similar. Because the EIS measurements were performed at the end of polarization step and their results were not extrapolated to the infinitively long duration of the polarization as in the case of the CA measurements, it could be expected that this agreement would be worse for these currents, which needed long time to stabilize. Indeed, the slowest stabilizations of the CA currents are observed in the range of polarizations between −0.15 and −0.25 V at p_{O2}=0.1 bar and for these data the discrepancies are the largest. This result corroborates that the oxygen electrode reaction at Au | YSZ interface is under the mixed control of the charge transfer and phenomenon induced by DC bias.

4 Conclusions

1. The CA and EIS measurements were performed at the Au | YSZ interface in the following ranges of the experimental parameters: potentials $-E$=0–0.3 V, partial pressures of oxygen p_{O2}=0.1–1.0 bar and temper-

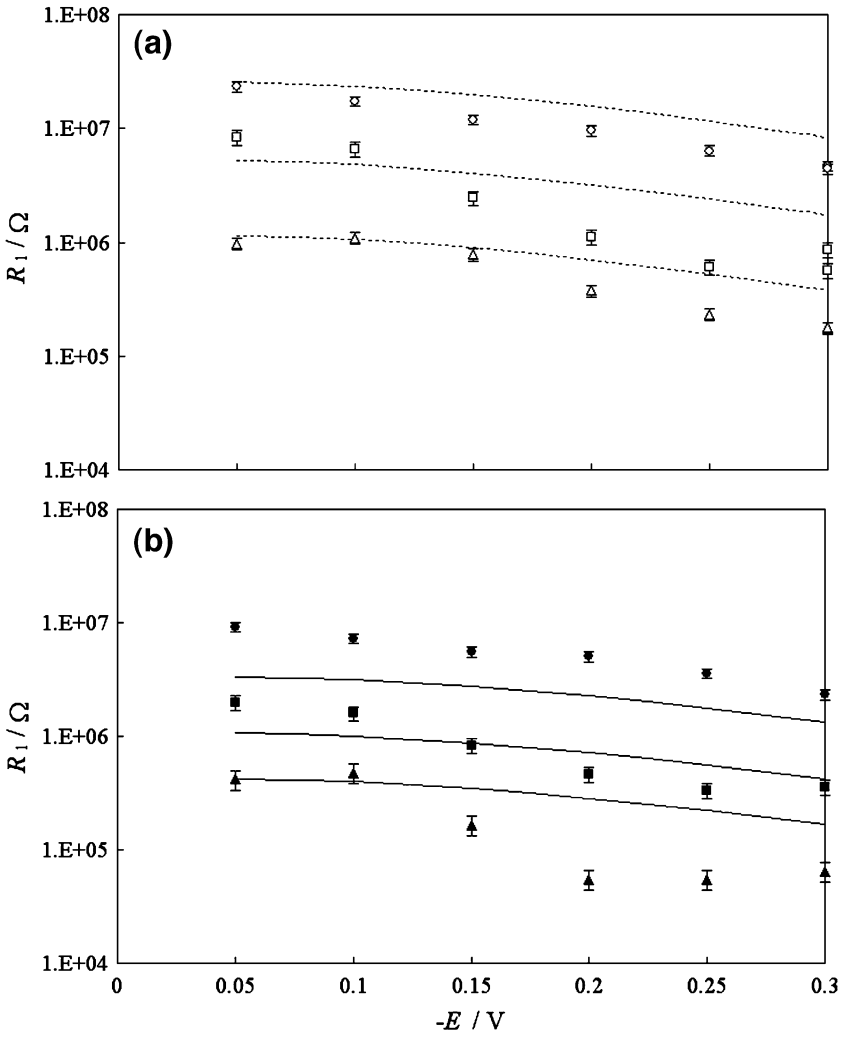

Fig. 12 Comparison of the apparent charge transfer resistances estimated by the CLNRS fit to the EIS responses (*points*) and calculated from Eqs. (5) and (6) with use of the data obtained on the basis of the CA measurements (*lines*). Au microelectrode at (**a**) 700 °C and (**b**) 800 °C. Partial pressure of oxygen p_{O2}: *unfilled circle*, *filled circle* 0.01 bar; *unfilled square*, *filled square* 0.1 bar and *unfilled triangle*, *filled triangle* 1 bar

atures 600–800 °C. It was shown that the three phase boundary length could be determined for the metallic microelectrode using the modified Newmann equation.
2. The CA experiments showed that the currents needed relatively long time to stabilize when the electrode was polarized with a constant negative potential lower than −0.15 V. Therefore, the estimation the asymptotic current, which corresponds to the infinitely long time of polarization, was evaluated to determine the apparent exchange currents and Tafel slopes.
3. The EIS characteristics of the polarized electrodes were measured after 15 h polarization. The relatively simply equivalent circuit, consisted of two parallel subcircuits R_1-*CPE* and R_2-*C,* was used to simulate the data obtained for the polarized Au microelectrodes. All the fitted parameters of the circuit elements remained virtually constant in the whole range of applied potentials apart the polarization resistance R_1. The further discussion justified that the oxygen electrode reaction at the Au | YSZ interface is under mixed control of the charge transfer and phenomenon induced by DC bias.

Acknowledgment One of the authors (PT) appreciates the financial support from the status founds 11.11.210.118.

References

1. M. Yashima, M. Kakihana, M. Yoshimura, Solid State Ion. **86–88**, 1131 (1996) DOI 10.1016/0167-2738(96)00386-4
2. O. Yamamoto, Electrochim. Acta. **45**, 2423 (2000) DOI 10.1016/S0013-4686(00)00330-3
3. W. Weppner, J. Solid State Chem. **20**, 305 (1977) DOI 10.1016/0022-4596(77)90167-0
4. M.F. Trubelja, V.S. Stubicam, Solid State Ion. **49**, 89 (1991) DOI 10.1016/0167-2738(91)90073-K
5. V.V. Kharton, F.M.B. Marques, A. Atkinson, in Fuel Cells Compendium, ed. by N.P. Brandon, D. Thompsett. *Transport Properties of Solid Oxide Electrolyte Ceramics; a Brief Review* (Elsevier, Amsterdam, 2005), p. 189
6. A. Mitterdorfer, L.J. Gauckler, Solid State Ion. **117**, 203 (1999) DOI 10.1016/S0167-2738(98)00340-3
7. S.N. Shkerin, S. Gormsen, S. Primdahl, M. Mogensen, Russ. J. Electrochem. **39**, 1058 (2003) DOI 10.1023/A:1026163118315
8. A.M. Svensson, S. Sunde, K. Nisancioglu, J. Electrochem. Soc. **145**, 1390 (1998) DOI 10.1149/1.1838471
9. S.B. Adler, Solid State Ion. **111**, 125 (1998) DOI 10.1016/S0167-2738(98)00179-9
10. J. Fleig, Solid oxide fuel cell cathodes: Polarization mechanisms and modelling of the electrochemical performance, in Annual Review of Material Research, 2003, v.33, p.361. DOI 10.1146/annurev.matsci.33.022802.093258
11. A. Parthasarathy, C.R. Martin, J. Electrochem. Soc. **138**, 916 (1991) DOI 10.1149/1.2085747
12. F.N. Büchi, M. Wakizoe, S. Srinivasan, J. Electrochem. Soc. **143**, 927 (1996) DOI 10.1149/1.1836560
13. P.D. Beattie, V.I. Basura, S. Holdcroft, J. Electroanal. Chem. **468**, 180 (1999) DOI 10.1016/S0022-0728(99)00164-3
14. S. Mitsushima, N. Araki, N. Kamiya, K. Ota, J. Electrochem. Soc. **149**, A1370 (2002) DOI 10.1149/1.1506164
15. J. Fleig, Solid State Ion. **161**, 279 (2003) DOI 10.1016/S0167-2738(03)00217-0
16. M.W. Breiter, K. Leeb, G. Fafilek, J. Electroanal. Chem. **434**, 129–137 (1997) DOI 10.1016/S0022-0728(97)00123-X
17. M.W. Breiter, K. Leeb, G. Fafilek, Electrochim. Acta. **43**, 325 (1998) DOI 10.1016/S0013-4686(97)00062-5
18. M. Sase, D. Ueno, K. Yashiro, A. Kaimai, T. Kawaga, J. Mizusaki, J. Phys.Chem. Solids. **66**, 343 (2005) DOI 10.1016/j.jpcs.2004.06.057
19. E. Ivers-Tiffée, A. Weber, K. Schmid, V. Krebs, Solid State Ion. **174**, 223 (2004) DOI 10.1016/j.ssi.2004.05.031
20. S.P. Jiang, J.G. Love, Solid State Ion. **138**, 183 (2001) DOI 10.1016/S0167-2738(00)00806-7
21. F.S. Baumann, J. Fleig, M. Konuma, U. Starke, H.-U. Habermeier, J. Maier, J. Electrochem. Soc. **152**, A2074 (2005) DOI 10.1149/1.2034529
22. X.J. Chen, K.A. Khor, S.H. Chan, Solid State Ion. **167**, 379 (2004) DOI 10.1016/j.ssi.2003.08.049
23. S.P. Jiang, J. Power Sources. **124**, 390 (2003) DOI 10.1016/S0378-7753(03)00814-0
24. W. Wang, S.P. Jiang, ECS Trans. **7**(1), 875 (2007)
25. J. Rutman, S. Raz, I. Riess, Solid State Ion. **177**, 1771 (2006) DOI 10.1016/j.ssi.2006.04.012
26. A. Hashibon, S. Raz, I. Riess, Solid Satate Ion. **149**, 167 (2002) DOI 10.1016/S0167-2738(02)00177-7
27. L. Bay, T. Jacobsen, Solid State Ion. **93**, 201 (1997) DOI 10.1016/S0167-2738(96)00526-7
28. T. Jacobsen, B. Zachau-Christiansen, L. Bay, M. Juhl Jørgensen, Electrochim. Acta. **46**, 1019 (2001) DOI 10.1016/S0013-4686(00)00689-7
29. T. Jacobsen, L. Bay, Electrochim. Acta. **47**, 2177 (2002) DOI 10.1016/S0013-4686(02)00094-4
30. J. Newman, J. Electrochem. Soc. **113**, 501 (1966) DOI 10.1149/1.2424003
31. A. Raźniak, P. Tomczyk, Materials Science (2008, in press). Available at http://www.materialsscience.pwr.wroc.pl/index.php?id=3&abst=62#a62
32. R.S. Nicholson, I. Shain, Anal. Chem. **36**, 706 (1964) DOI 10.1021/ac60210a007
33. J.M. Saveant, E. Vianello, ed. by J.S. Longmuir. *Advances in Polarography*, vol.1 (Pergamon, NY, 1960), p. 367
34. R.S. Nicholson, I. Shain, Anal. Chem. **36**, 706 (1964) DOI 10.1021/ac60210a007
35. L. Rampazzo, J. Electroanal. Chem. **14**, 117 (1967) DOI 10.1016/0022-0728(67)80137-2
36. P.A. Allen, A. Hickling, Trans. Faraday Soc. **53**, 1626 (1957) DOI 10.1039/tf9575301626
37. N.Q. Minh, J. Am. Ceram. Soc. **76**, 563 (1993) DOI 10.1111/j.1151-2916.1993.tb03645.x
38. J.F. Baumard, P. Abelard, in Advances in Ceramics, vol. 12, ed. by N. Claussen, M. Rühle, A.H. Heurer. *Defect Structure and Transport Properties of ZrO_2-Based Electrolytes* (American Ceramic, Coloumbus, OH, 1984), p. 555
39. Fuel Cell Handbook. 5th edition by EG&G Services Parsons Inc., Science Application International Corporation (US Department of Energy, Morgantown, 2000), p.8–5